
LIMITED MEMORY LRSGA OPTIMIZER TO COMPETITIVE OPTIMIZATION

A PREPRINT

Katherine Rossella Foglia*

Department of Mathematics and Computer Science
University of Calabria
Rende (CS), 87036, Italy
katherine.foglia@unical.it

Francesco Sergio Pisani†

Institute for High Performance Computing and Networking
Italian National Research Council
Rende (CS), 87036, Italy
francescosergio.pisani@icar.cnr.it

Vittorio Colao‡

Department of Mathematics and Computer Science
University of Calabria
Rende (CS), 87036, Italy
vittorio.colao@unical.it

ABSTRACT

We introduce LM-LRSGA, a limited-memory variant of Low-Rank Symplectic Gradient Adjustment (LRSGA) for differentiable games. It is an iterative scheme for approximating Nash equilibria at first-order cost while preserving the stabilizing benefits of second-order information. By storing only a limited history of curvature pairs, LM-LRSGA is well suited to high-parameter competitive models such as GANs.

Keywords Nash equilibria · Competitive optimization · GreenAI · Limited memory · Spectral analysis

1 Introduction

Optimization in multi-agent and adversarial settings is a central challenge in modern machine learning. Examples include Generative Adversarial Networks (GANs), adversarial training for robustness, and multi-agent reinforcement learning, where two or more agents optimize distinct, often conflicting objectives.

These problems can be viewed as differentiable games: each agent minimizes its own objective. Despite the similarity to classical optimization, the coupled objectives and the lack of a single potential make the dynamics fundamentally different. Even in the two-player case, gradient methods may cycle, oscillate, or diverge rather than converge to equilibrium Arjovsky et al. [2017], M Wiatrak [2019], Balduzzi et al. [2018].

Formally, for the two-player setting, we denote by $x \in \mathbb{R}^m$ and $y \in \mathbb{R}^n$ the strategy variables for Players 1 and 2, and by $f, g : \mathbb{R}^{m+n} \rightarrow \mathbb{R}$ the corresponding payoff functions.

A Nash equilibrium (x^*, y^*) is a pair where neither player can locally improve its objective, holding the other fixed. For differentiable f and g , the first-order conditions are

$$\partial_x f(x^*, y^*) = 0, \quad \partial_y g(x^*, y^*) = 0. \quad (1)$$

*Department of Mathematics and Computer Science, University of Calabria, Ponte P. Bucci, 30B, Arcavacata di Rende (CS), 87036, Italy. katherine.foglia@unical.it

†Institute for High Performance Computing and Networking, Italian National Research Council, Via P. Bucci 8/9C, Arcavacata di Rende (CS), 87036, Italy. francescosergio.pisani@icar.cnr.it

‡Department of Mathematics and Computer Science, University of Calabria, Ponte P. Bucci, 30B, Arcavacata di Rende (CS), 87036, Italy vittorio.colao@unical.it

Stacking $w = (x, y) \in \mathbb{R}^{m+n}$, the game gradient is defined as

$$F(w) = \begin{pmatrix} \partial_x f(w) \\ \partial_y g(w) \end{pmatrix},$$

so that equilibria satisfy $F(w^*) = 0$. This generalizes single-objective optimization to a vector field, but here F is typically non-conservative and non-monotone, so standard convex tools do not apply in general.

Understanding the underlying geometry is therefore crucial. The Jacobian of F , i.e., the game Hessian,

$$H(w) = \begin{pmatrix} \partial_{xx}^2 f(w) & \partial_{xy}^2 f(w) \\ \partial_{yx}^2 g(w) & \partial_{yy}^2 g(w) \end{pmatrix},$$

admits the decomposition $H = S + A$ with symmetric $S = \frac{1}{2}(H + H^\top)$ and antisymmetric $A = \frac{1}{2}(H - H^\top)$. The part S drives motion toward equilibria, while A induces rotational or Hamiltonian-like components that prevent convergence. Prior work Balduzzi et al. [2018], Gemp and Mahadevan [2018] shows that unmitigated rotations cause simultaneous gradient descent to behave as a non-dissipative dynamical system; even in the bilinear game $\Phi(x, y) = x^\top y$,

$$x_{n+1} = x_n - \eta \partial_x f(x_n, y_n), \quad y_{n+1} = y_n - \eta \partial_y g(x_n, y_n)$$

generates limit cycles (see also Schäfer and Anandkumar [2019]). These rotations arise from antisymmetric interactions between players' gradients and behave like a skew-symmetric force field. In continuous time, dynamics resemble Hamiltonian systems: energy is conserved, producing a potential (gradient) component toward equilibria and a rotational flow around them. Hence, restoring convergence requires damping or correcting the antisymmetric part.

This insight motivated algorithms with second-order corrections, symplectic damping, or predictive steps. The Symplectic Gradient Adjustment (SGA) Balduzzi et al. [2018] preconditions updates with $(I - \tau A(w))$, counteracting rotation and stabilizing trajectories near equilibria. The Optimistic Gradient method Daskalakis and Panageas [2018] and the Extragradient technique Korpelevich [1976], Gidel et al. [2019] exploit the variational structure of the problem to capture and correct the cycling behaviour. Finally, Competitive Gradient Descent (CGD) Schäfer and Anandkumar [2019] interprets game optimization through a local bilinear model whose Nash equilibrium defines a stable update. However, many of these methods are costly: explicit or implicit mixed second-order derivatives scale poorly. Even for moderate networks, forming $\partial_{xy}^2 f$ and $\partial_{yx}^2 g$ is impractical. Quasi-Newton approximations mitigate this: BFGS/L-BFGS Nocedal [1980], Liu and Nocedal [1989] maintain low-rank curvature via secant updates, achieving near-second-order behavior at first-order cost. Building on this, Low-Rank SGA (LRSGA) Vater et al. [2025] replaces mixed derivatives with low-rank secant updates, recovering much of SGA's stabilization without full Hessian storage. Yet the low-rank factors still require memory that grows with problem dimension, which can become prohibitive for large models.

We address this scalability bottleneck with *Limited-Memory Low-Rank Symplectic Gradient Adjustment* (LM-LRSGA). The method combines symplectic gradient corrections with L-BFGS-style recursions: instead of storing dense factors, it keeps a short history of curvature pairs capturing essential information from recent iterates. Modified two-loop recursion algorithms compute the LRSGA products implicitly, avoiding matrix formation or storage. Thus LM-LRSGA preserves LRSGA's stabilizing effect while using linear memory and first-order-like per-step complexity, making it suitable for large-scale adversarial/stochastic settings (e.g., GANs with millions of parameters).

We validate the approach on GAN training over MNIST and Fashion-MNIST, comparing LM-LRSGA against the Adam Kingma and Ba [2014] optimizer. Empirically, LM-LRSGA yields more stable training dynamics and faster convergence, with smooth and synchronized loss trajectories for both generator and discriminator. Quantitatively, it improves Fréchet Inception Distance (FID) by up to 30% over Adam while maintaining comparable computational cost. Sensitivity analyses show robustness to learning rate, history length, and damping factors, highlighting suitability for large-scale and stochastic regimes.

Beyond computation, the method supports sustainable ML: by avoiding explicit second-order computation and reducing memory footprint, LM-LRSGA lowers training time, suggesting efficiency and environmental friendliness.

The rest of the paper is organized as follows.

Section 2 reviews competitive optimization and recalls SGA and LRSGA. Section 3 presents LM-LRSGA, detailing its two-loop recursion algorithms and update rules. Section 4 reports experiments on GANs trained on MNIST and Fashion-MNIST, and presents sensitivity analyses. Section 6 concludes and outlines potential future extensions to large-scale stochastic and distributed settings.

2 Preliminaries and Mathematical Framework

Let $X \subset \mathbb{R}^m$ and $Y \subset \mathbb{R}^n$ be nonempty, convex and compact subsets, and $\Omega \subset \mathbb{R}^{m+n}$ open and convex such that $X \times Y \subset \Omega$. Let $f, g \in C^3(\Omega, \mathbb{R})$ be two objective functions. A two-player competitive optimization problem, where

Player 1 (with strategy x) and Player 2 (with strategy y) aim to minimize their respective objective functions f and g , can be written as:

$$\min_{x \in X} f(x, y) \quad \min_{y \in Y} g(x, y). \quad (2)$$

Solutions to problem 2 are called Nash equilibria (NE) and denoted by (x^*, y^*) . For a shorter notation, we write $w = (x, y) \in X \times Y$. The first-order stationarity and the second-order necessary conditions for a local NE are:

$$F(w^*) = 0, \quad \partial_{xx}^2 f(w^*) \succeq 0, \quad \partial_{yy}^2 g(w^*) \succeq 0. \quad (3)$$

Moreover, to ensure that the NE is isolated and locally stable, we assume $H(w^*)$ to be invertible and semi-definite positive i.e. $\langle z, H(w^{\text{NE}}) z \rangle \geq 0$ for all $z \in \mathbb{R}^{m+n}$.

We remark that the game Hessian matrix admits the symmetric/antisymmetric decomposition

$$S(x, y) = \frac{H(x, y) + H(x, y)^\top}{2}, \quad A(x, y) = \frac{H(x, y) - H(x, y)^\top}{2}.$$

As reported in the literature Balduzzi et al. [2018], the antisymmetric component $A(x, y)$ is directly responsible for rotational/oscillatory dynamics during training, which can delay or even prevent rapid convergence to equilibria.

To counteract such phenomena, the *Symplectic Gradient Adjustment* (SGA) method introduced in Balduzzi et al. [2018] modifies the descent direction by subtracting the rotational component induced by A . Its update rule is

$$w_{k+1} = w_k - \eta (I - \tau A(w_k)) F(w_k),$$

where I represents the identity matrix in the appropriate Euclidean space, $w_k := (x_k, y_k)$ the iterate k , $\eta > 0$ the stepsize and $\tau > 0$ controls the strength of the antisymmetric correction. The antisymmetric component of the game Hessian at iterate w_k $A(w_k)$ has the block form:

$$A(w_k) = \begin{pmatrix} 0_m & \frac{1}{2} (\partial_{xy}^2 f(w_k) - \partial_{yx}^2 g(w_k)^\top) \\ \frac{1}{2} (\partial_{yx}^2 g(w_k) - \partial_{xy}^2 f(w_k)^\top) & 0_n \end{pmatrix} \quad (4)$$

As outlined in the introduction, our recent variant—*Low-Rank Symplectic Gradient Adjustment* (LRSGA)—proposed in Vater et al. [2025], addresses the high computational cost of explicitly forming the mixed second derivatives $\partial_{xy}^2 f(x, y)$ and $\partial_{yx}^2 g(x, y)$ by employing Broyden’s least-change (rank-one) secant updates Broyden [1965] to obtain efficient approximations of these mixed blocks. In particular, we maintain Broyden-type Jacobian estimates with $\mu_k \approx (\partial_{xx}^2 f \mid \partial_{xy}^2 f) \in \mathbb{R}^{m \times (m+n)}$ and $\nu_k \approx (\partial_{yx}^2 g \mid \partial_{yy}^2 g) \in \mathbb{R}^{n \times (m+n)}$. Henceforth we retain only the mixed-derivative block-columns, denoted $[\mu_k]_2$ and $[\nu_k]_1$, which approximate $\partial_{xy}^2 f$ and $\partial_{yx}^2 g$, respectively.

It is algebraically and computationally equivalent (at the level of per-iteration arithmetic) to (i) form μ_k and ν_k and then extract only the mixed blocks $[\mu_k]_2$ and $[\nu_k]_1$, or (ii) update directly the mixed blocks. Indeed, starting from (5) and partitioning $\mu_k = ([\mu_k]_1 \mid [\mu_k]_2)$ and $\nu_k = ([\nu_k]_1 \mid [\nu_k]_2)$, one readily verifies

$$[\mu_{k+1}]_2 = [\mu_k]_2 + \frac{(\partial_x f_{k+1} - \partial_x f_k - [\mu_k]_1(x_{k+1} - x_k) - [\mu_k]_2(y_{k+1} - y_k))(y_{k+1} - y_k)^\top}{(w_{k+1} - w_k)^\top (w_{k+1} - w_k)} \quad (5)$$

$$[\nu_{k+1}]_1 = [\nu_k]_1 + \frac{(\partial_y g_{k+1} - \partial_y g_k - [\nu_k]_2(y_{k+1} - y_k) - [\nu_k]_1(x_{k+1} - x_k))(x_{k+1} - x_k)^\top}{(w_{k+1} - w_k)^\top (w_{k+1} - w_k)} \quad (6)$$

where $f_k := f(w_k)$ and $g_k := g(w_k)$. Note that

$$(w_{k+1} - w_k)^\top (w_{k+1} - w_k) = \|x_{k+1} - x_k\|_2^2 + \|y_{k+1} - y_k\|_2^2.$$

Thus, in either formulation the same quantities—namely the products $[\mu_k]_1(x_{k+1} - x_k)$ and $[\nu_k]_2(y_{k+1} - y_k)$ —are required, and the per-step computational cost is comparable. Moreover, near a stable Nash equilibria w^* , the own-player Hessian blocks are assumed to be positive semidefinite by the second-order necessary conditions of Nash equilibria point:

$$\partial_{xx}^2 f(w^*) \succeq 0, \quad \partial_{yy}^2 g(w^*) \succeq 0.$$

We can assume moreover that these blocks are uniformly bounded in a convex neighborhood Ω of w^* :

$$0 \preceq \partial_{xx}^2 f(w) \preceq \bar{\lambda}_x I_m, \quad 0 \preceq \partial_{yy}^2 g(w) \preceq \bar{\lambda}_y I_n, \quad \forall w \in \Omega. \quad (7)$$

(These bounds follow, e.g., from continuity of the Hessians plus compactness of Ω .) Under (7) it is consistent to replace the unknown diagonal blocks by $\varepsilon_x I_m$ and $\varepsilon_y I_n$, with

$$0 \leq \varepsilon_x \leq \bar{\lambda}_x, \quad 0 \leq \varepsilon_y \leq \bar{\lambda}_y,$$

which allow us to consider:

$$\begin{aligned} M_{k+1} &= M_k + \frac{(\partial_x f_{k+1} - \partial_x f_k - \varepsilon_x(x_{k+1} - x_k) - M_k(y_{k+1} - y_k))(y_{k+1} - y_k)^\top}{(w_{k+1} - w_k)^\top (w_{k+1} - w_k)} \\ N_{k+1} &= N_k + \frac{(\partial_y g_{k+1} - \partial_y g_k - \varepsilon_y(y_{k+1} - y_k) - N_k(x_{k+1} - x_k))(x_{k+1} - x_k)^\top}{(w_{k+1} - w_k)^\top (w_{k+1} - w_k)} \end{aligned} \quad (8)$$

The induced modeling error in the secant residuals remains bounded and can be made small by choosing $\varepsilon_x, \varepsilon_y$ within the spectral bounds in (7). Practically, $\varepsilon_x, \varepsilon_y$ play the role of Tikhonov/Levenberg–Marquardt regularization; setting them to 0 corresponds to ignoring the diagonal blocks, whereas small positive values improve stability without increasing memory.

Therefore, the (slightly revised) LRSGA we employ adopts the following iterative rule:

$$w_{k+1} = w_k - \eta (I - \tau \alpha_k) F(w_k), \quad (9)$$

where

$$\alpha_k = \begin{pmatrix} 0 & \frac{1}{2}(M_k - N_k^\top) \\ \frac{1}{2}(N_k - M_k^\top) & 0 \end{pmatrix} \approx A(w_k). \quad (10)$$

This work introduces a *Limited-Memory LRSGA (LM-LRSGA)* variant that preserves the theoretical framework of LRSGA while avoiding the explicit storage of the matrices M_k and N_k . The implementation follows a *two-loop recursion* scheme in the spirit of L-BFGS Nocedal [1980], Liu and Nocedal [1989], leading to substantial memory savings and making the method suitable for large-scale competitive settings. Further details and evidence are provided in the subsequent sections.

3 Limited Memory LRSGA

As highlighted, LRSGA requires storing the matrices M_k and N_k to approximate the mixed second derivatives, which can be memory-intensive for high-dimensional models. To address this, we propose a *Limited-Memory LRSGA* variant that preserves LRSGA’s theoretical robustness while substantially reducing memory usage.

Our strategy follows the *two-loop recursion* method, successfully employed by L-BFGS Nocedal [1980], Liu and Nocedal [1989]. The key idea is to avoid storing the full updated matrices M_k and N_k ; instead, we retain only the most recent ℓ pairs among the four vectors $\{s_k^x, s_k^y, y_k^f, y_k^g\}$, defined as

$$\begin{aligned} s_k^x &= x_k - x_{k-1}, & s_k^y &= y_k - y_{k-1}, \\ y_k^f &= \partial_x f(w_k) - \partial_x f(w_{k-1}) - \varepsilon_x s_k^x, & y_k^g &= \partial_y g(w_k) - \partial_y g(w_{k-1}) - \varepsilon_y s_k^y. \end{aligned}$$

Adopting this notation and denoting $s_k^w := (s_k^x, s_k^y)$, LRSGA can be written as follows:

Algorithm 1 LRSGA (Low-Rank Symplectic Gradient Adjustment)

- 1: **Phase 1: Gradient Computation and Update**
 - 2: **for** $k = 1, 2, \dots$ **do**
 - 3: $M_{k+1} \leftarrow M_k + \frac{(y_k^f - M_k s_k^y)}{(s_k^w)^\top s_k^w} (s_k^y)^\top$
 - 4: $N_{k+1} \leftarrow N_k + \frac{(y_k^g - N_k s_k^x)}{(s_k^w)^\top s_k^w} (s_k^x)^\top$
 - 5: $x_{k+1} \leftarrow x_k - \eta \left(\partial_x f(w_k) - \frac{\tau}{2} (M_k - N_k^\top) \right) \partial_y g_k$
 - 6: $y_{k+1} \leftarrow y_k - \eta \left(\partial_y g(w_k) - \frac{\tau}{2} (N_k - M_k^\top) \right) \partial_x f_k$
 - 7: **end for**
 - 8: **Output:** Updated x_k and y_k until convergence.
-

3.1 Limited-memory recursive updates for M_k and N_k

The updates for the matrices M_k and N_k can be written in a limited-memory, iterative form by storing only the last ℓ pairs (s_t, y_t) and using the auxiliary matrices

$$\tilde{V}_k := I - p_k s_k^y (s_k^y)^\top, \quad V_k := I - p_k s_k^x (s_k^x)^\top,$$

with

$$p_k := \frac{1}{(s_k^w)^\top s_k^w}.$$

Consequently, iterations 8 can be rewrite as:

$$M_k = M_{k-1} \tilde{V}_{k-1} + p_{k-1} y_{k-1}^f (s_{k-1}^y)^\top \quad \text{and} \quad N_k = N_{k-1} V_{k-1} + p_{k-1} y_{k-1}^g (s_{k-1}^x)^\top$$

By considering only the last ℓ pairs (s_t, y_t) , these became:

$$\begin{aligned} M_k &= M_{k-\ell} (\tilde{V}_{k-\ell} \dots \tilde{V}_{k-1}) + p_{k-\ell} y_{k-\ell}^f (s_{k-\ell}^y)^\top (\tilde{V}_{k-\ell+1} \dots \tilde{V}_{k-1}) + \dots \\ &\quad + p_{k-2} y_{k-2}^f (s_{k-2}^y)^\top \tilde{V}_{k-1} + p_{k-1} y_{k-1}^f (s_{k-1}^y)^\top, \\ N_k &= N_{k-\ell} (V_{k-\ell} \dots V_{k-1}) + p_{k-\ell} y_{k-\ell}^g (s_{k-\ell}^x)^\top (V_{k-\ell+1} \dots V_{k-1}) + \dots \\ &\quad + p_{k-2} y_{k-2}^g (s_{k-2}^x)^\top V_{k-1} + p_{k-1} y_{k-1}^g (s_{k-1}^x)^\top. \end{aligned}$$

By symmetry of the projectors ($\tilde{V}_t = \tilde{V}_t^\top$ and $V_t = V_t^\top$), the compact transposed forms read:

$$M_k^\top = \left(\tilde{V}_{k-1} \dots \tilde{V}_{k-\ell} \right) (M_{(k-\ell)})^\top + p_{k-\ell}^y \left(\tilde{V}_{k-1} \dots \tilde{V}_{k-\ell+1} \right) s_{k-\ell}^y (y_{k-\ell}^f)^\top + \dots + p_{k-1}^y s_{k-1}^y (y_{k-1}^f)^\top,$$

and, analogously,

$$N_k^\top = \left(V_{k-1} \dots V_{k-\ell} \right) (N_{(k-\ell)})^\top + p_{k-\ell}^x \left(V_{k-1} \dots V_{k-\ell+1} \right) s_{k-\ell}^x (y_{k-\ell}^g)^\top + \dots + p_{k-1}^x s_{k-1}^x (y_{k-1}^g)^\top.$$

These representations enable the computation of the four products required by LRSQA—namely $M_k \partial_y g(w_k)$, $N_k^\top \partial_y g(w_k)$, $N_k \partial_x f(w_k)$, $M_k^\top \partial_x f(w_k)$ —while substantially reducing the memory footprint.

3.2 Adapted two-loop recursion algorithms

Classical L-BFGS uses the two-loop recursion to apply a *square* (inverse) Hessian approximation $H_k \in \mathbb{R}^{d \times d}$ to a vector. In contrast, our setting requires multiplying *rectangular* mixed-Jacobian approximation and their transpositions, $M_k \in \mathbb{R}^{m \times n}$ and $N_k \in \mathbb{R}^{n \times m}$, by vectors of compatible size. To this end, we adapt the recursion by storing the ℓ pairs $\{(s_t^y, y_t^f)\}$ and $\{(s_t^x, y_t^g)\}$, and by using side-specific projectors $\tilde{V}_t := I - p_t s_t^y (s_t^y)^\top$ and $V_t := I - p_t s_t^x (s_t^x)^\top$, with the common scaling $p_t := 1/\|(s_t^w)\|_2^2$. This preserves the appropriate secant conditions for the *mixed* blocks while avoiding storage of the full matrices.

3.2.1 Direct Two-loop recursion

Given a generic vector q , we can compute $M_k q$ and $N_k q$ via the Algorithm 2 below.

Algorithm 2 TwoLoopRecursionDirect-K

- 1: **Input:** $\{p_{k-1}, p_{k-2}, \dots, p_{k-\ell}\}, \{s_{k-1}^j, s_{k-2}^j, \dots, s_{k-\ell}^j\}, \{y_{k-1}^h, y_{k-2}^h, \dots, y_{k-\ell}^h\}, j \in \{x, y\}, h \in \{f, g\}$, vettore q , matrice iniziale H_0^k
 - 2: **for** $i = k-1, k-2, \dots, k-\ell$ **do**
 - 3: $\alpha_i \leftarrow p_i (s_i^j)^\top q$
 - 4: $q \leftarrow q - \alpha_i s_i^j$
 - 5: **end for**
 - 6: $r \leftarrow H_0^k q$
 - 7: **for** $i = k-\ell, k-\ell+1, \dots, k-1$ **do**
 - 8: $r \leftarrow r + y_i^h \alpha_i$
 - 9: **end for**
 - 10: **Output:** r
-

Applying Algorithm 2 with the appropriate inputs yields the LRSGA products:

$$M_k \partial_y g(w_k) = \mathbf{TwoLoopRecursionDirect-K}(\{p_t, s_t^y, y_t^f\}_{t=k-\ell}^{k-1}, q = \partial_y g(w_k), H_0^k = M_{k-\ell}),$$

$$N_k \partial_x f(w_k) = \mathbf{TwoLoopRecursionDirect-K}(\{p_t, s_t^x, y_t^g\}_{t=k-\ell}^{k-1}, q = \partial_x f(w_k), H_0^k = N_{k-\ell}).$$

3.2.2 Transpose Two-loop recursion

Given a vector q , to compute products $M_k^\top q$ and $N_k^\top q$, we use the following limited-memory transpose recursions that mirror the direct case.

Algorithm 3 TwoLoopRecursionTranspose-K

```

1: Input:  $\{p_{k-1}, p_{k-2}, \dots, p_{k-\ell}\}, \{s_{k-1}^j, s_{k-2}^j, \dots, s_{k-\ell}^j\}, \{y_{k-1}^h, y_{k-2}^h, \dots, y_{k-\ell}^h\}, j \in \{x, y\}, h \in \{f, g\}$ , vector
    $q$ , initial matrix  $(H_0^k)^\top$ 
2: for  $i = k-1, k-2, \dots, k-\ell$  do
3:    $\alpha_i \leftarrow p_i (y_i^h)^\top q$ 
4: end for
5:  $r \leftarrow (H_0^k)^\top q$ 
6: for  $i = k-\ell, k-\ell+1, \dots, k-1$  do
7:    $\beta_i \leftarrow p_i (s_i^j)^\top r$ 
8:    $r \leftarrow r + s_i^j (\alpha_i - \beta_i)$ 
9: end for
10: Output:  $r$ 

```

In particular, we apply Algorithm 3, as follows:

$$M_k^\top \partial_x f(w_k) = \mathbf{TwoLoopRecursionTranspose-K}(\{p_t, s_t^y, y_t^f\}_{t=k-\ell}^{k-1}, q = \partial_x f(w_k), H_0^k = (M_{k-\ell})^\top),$$

$$N_k^\top \partial_y g(w_k) = \mathbf{TwoLoopRecursionTranspose-K}(\{p_t, s_t^x, y_t^g\}_{t=k-\ell}^{k-1}, q = \partial_y g(w_k), H_0^k = (N_{k-\ell})^\top).$$

Finally, to avoid storing a full base matrix H_0^k (and its transpose) in the two-loop recursions, we set

$$H_0^k := \frac{y_{k-\ell-1}^h (s_{k-\ell-1}^j)^\top}{(s_{k-\ell-1})^\top (s_{k-\ell-1})},$$

where $j \in \{x, y\}$ and $h \in \{f, g\}$ matches the recursion (i.e., $j = y$ and $h = f$ for the M_k -recursion, and $j = x$, $h = g$ for the N_k -recursion and $s_t = (s_t^x, s_t^y)$ is the joint vector. With this rank-one choice, matrix-vector products reduce to inner products:

$$H_k^0 q = \frac{y_{k-1}^h ((s_{k-1}^j)^\top q)}{(s_{k-1})^\top (s_{k-1})}, \quad (H_k^0)^\top q = \frac{s_{k-1}^j ((y_{k-1}^h)^\top q)}{(y_{k-1}^h)^\top (y_{k-1}^h)}.$$

We remark that in both differences $\partial_x f(w_{k+1}) - \partial_x f(w_k)$ and $\partial_y g(w_{k+1}) - \partial_y g(w_k)$ relate two consecutive iterates and this implies that each term is evaluated on the *current* mini-batch k (e.g., $\partial_x f_{B_{k+1}}(w_{k+1}) - \partial_x f_{B_k}(w_k)$). We emphasize that this fact degrades the accuracy of the mixed-second-derivative approximations used by our secant updates and so a stochastic implementation is required.

In line with stochastic quasi-Newton practice Guo et al. [2023], we therefore adopt *gradient displacement* (also called common/consistent-batch): both gradients in each difference are computed on the *same* mini-batch, i.e.,

$$\partial_x f_{B_k}(w_{k+1}) - \partial_x f_{B_k}(w_k), \quad \partial_y g_{B_k}(w_{k+1}) - \partial_y g_{B_k}(w_k),$$

which reduces variance and preserves secant consistency for the mixed blocks. As an alternative, one may enforce overlapping mini-batches with $I_k := B_k \cap B_{k+1} \neq \emptyset$ and form the differences on the intersection,

$$\partial_x f_{I_k}(w_{k+1}) - \partial_x f_{I_k}(w_k), \quad \partial_y g_{I_k}(w_{k+1}) - \partial_y g_{I_k}(w_k).$$

We propose an additional variant, **LM-LRSGA-EMA**, which mitigates mini-batch-induced noise without manipulating the batches. Specifically, we maintain exponential moving averages of y_k^f and y_k^g and use them in the two-loop recursions:

$$\tilde{y}_k^f = \beta \tilde{y}_{k-1}^f + (1 - \beta) y_k^f, \quad \tilde{y}_k^g = \beta \tilde{y}_{k-1}^g + (1 - \beta) y_k^g, \quad \beta \in [0, 1),$$

replacing y_k^f, y_k^g with $\tilde{y}_k^f, \tilde{y}_k^g$ in the update formulas. This EMA version seems to reduce variance, and improves stability without altering the underlying dynamics.

In conclusion, the proposed approach computes LRSGA updates with a markedly reduced memory footprint, thereby substantially broadening its applicability to high-dimensional models.

In the next section, we present experiments on generative adversarial networks (GANs), benchmarking against the widely used Adam optimizer, to empirically assess the advantages of the Limited-Memory LRSGA (LM-LRSGA) variant.

4 Experimental results

Using two benchmark datasets, we have measured the performance of our algorithm comparing with the well known Adam optimizer. Regarding the constraint of using a competitive environment, we choose the Generative Adversarial Networks (GANs) model that has two models trained in a competitive manner, the performance of an optimizer is determined by its ability to balance the dynamics between two adversarial objectives: the generator goal of producing realistic outputs and the discriminator goal of correctly distinguishing between real and generated samples. This setting is inherently unstable, as improvements in one model performance can degrade the other, leading to oscillations or divergence if the optimization is not well controlled. In the standard GAN formulation, the discriminator D seeks to maximize the classification accuracy between real data $x \sim p_{\text{data}}$ and generated samples $G(z)$ from latent variables $z \sim p_z$ (i.e., randomly sampled from a uniform distribution), while the generator G aims to minimize the same objective to “fool” the discriminator. Formally, the discriminator loss is given by

$$\mathcal{L}_D = -\mathbb{E}_{x \sim p_{\text{data}}} [\log D(x)] - \mathbb{E}_{z \sim p_z} [\log (1 - D(G(z)))],$$

and the generator loss by

$$\mathcal{L}_G = -\mathbb{E}_{z \sim p_z} [\log D(G(z))] + \lambda \|\theta_G\|$$

where the λ term weights the penalty component for the G parameters.

An effective optimizer in this context must maintain a delicate equilibrium, ensuring that neither the generator nor the discriminator overpowers the other, thereby facilitating stable training and yielding high-quality, realistic outputs over time.

We have analyzed the shape of the losses to understand the ability of the optimizer to minimize and maximize the training objectives. Also, we present a quality metric to understand how the trained model is able to generate realistic images. In this context, the term “realistic” refers to the ability of generating images similar to real data. The Fréchet Inception Distance (FID) score is a widely used metric for evaluating the quality of images generated by generative models such as GANs. It measures the similarity between the distribution of generated images and that of real images by comparing the mean and covariance of feature representations extracted from a pretrained Inception network. Mathematically, lower FID values indicate that the generated images are more similar to real ones in terms of both visual quality and diversity, with zero representing a perfect match.

4.1 Experiment on Mnist

The first experiment is conducted on the MNIST dataset, a classic benchmark in machine learning and computer vision, consisting of 70,000 grayscale images of handwritten digits from 0 to 9. Each image is 28×28 pixels and centered within the frame to standardize positioning. The data set is divided into 60,000 training samples and 10,000 test samples, and its simplicity, small size, and well-defined labels have made it a fundamental starting point for testing and comparing classification algorithms. We used only the training split to train the GAN.

4.1.1 Results

Figure 1a presents the Fréchet Inception Distance (FID) scores over training epochs on the MNIST dataset. It compares our proposed optimizer LM-LRSGA, and its exponential moving average variant (LRSGAema) against the widely

used Adam optimizer. Both LM-LM-LRSGA and LM-LRSGAema achieve substantially lower FID scores throughout training than Adam, demonstrating superior sample quality. While Adam begins with a significantly higher FID score (above 70) and gradually decreases to around 19 after 100 epochs, LM-LRSGA and LM-LRSGAema start with lower scores (~ 45) and converge much faster. Notably, LM-LRSGAema consistently outperforms LRSGA, yielding smoother convergence and the lowest final FID score of approximately 13. These results highlight the effectiveness of our optimizer in stabilizing generative model training and producing higher-quality samples compared to the conventional Adam baseline.

Figure 1b shows the generator and discriminator loss trajectories on the MNIST dataset when trained with LRSGA, LM-LRSGAema, and Adam. The results indicate that LM-LRSGA and LM-LRSGAema lead to more stable and balanced adversarial training than Adam. With Adam, the generator loss remains consistently lower (~ 1.3) while the discriminator stabilizes around ~ 0.8 , reflecting a tendency toward imbalance and potential mode collapse. In contrast, LM-LRSGA and LM-LRSGAema exhibit more synchronized dynamics: the generator loss converges to ~ 1.4 , while the discriminator loss steadily decreases toward ~ 0.5 , suggesting healthier competition between the two networks. Notably, LM-LRSGAema achieves the smoothest convergence, stabilizing both losses earlier and exhibiting minimal oscillation. These findings align with the FID results, demonstrating that our proposed optimizer fosters more stable GAN training and enhances generative performance relative to the Adam baseline.

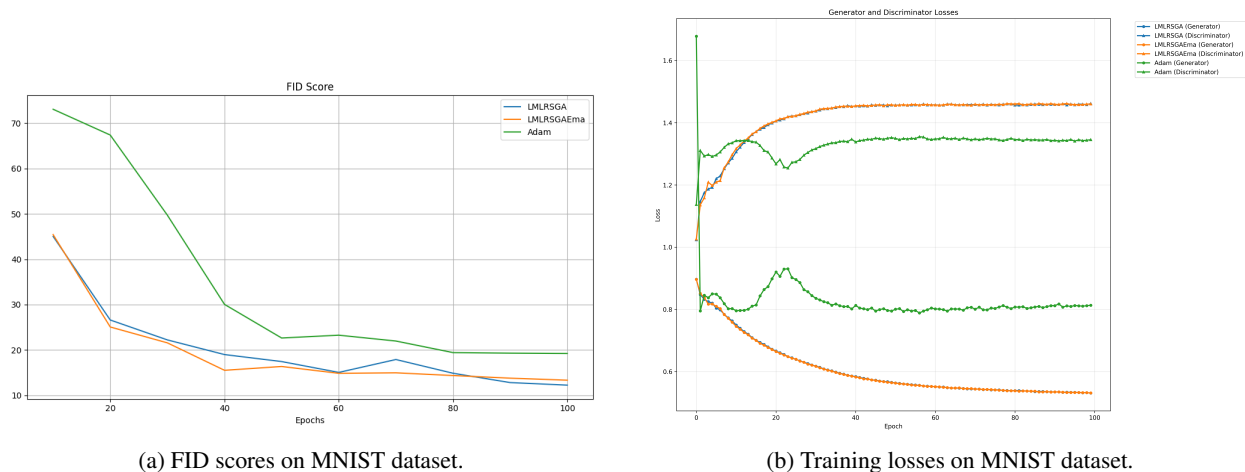


Figure 1: Comparison of LM-LRSGAema and Adam optimizers on MNIST datasets.

4.1.2 Sensitivity analysis

In this section, we analyze the role of the main parameters of the LRMSGAEma algorithm. We studied how the model ability generates realistic images when we change the value of a parameter.

Figure 2a presents the hyperparameter sensitivity analysis η on the minimum Fréchet Inception Distance (FID) score achieved during the experiments. The bar chart shows results for η values ranging from 0.05 to 0.30. Performance varies notably across settings, with the highest (worst) FID score observed at $\eta = 0.05$, indicating degraded generative quality in this regime. The best results are obtained for η values between 0.20 and 0.25, yielding minimum FID scores around 14, suggesting an optimal trade-off between learning stability and image fidelity. Larger η values beyond 0.25 slightly worsen the FID, though still outperforming the smallest η tested. This pattern highlights the importance of tuning η for maximizing GAN performance.

Figure 2b reports the hyperparameter sensitivity analysis for the parameter τ . The results are shown for τ values from 0 to 0.2. The 0 value is an experiment in which the component is ignored. Across this range, the minimum FID scores vary only slightly, indicating that the model performance is relatively insensitive to τ within the tested limits. The best generative quality is observed at $\tau = 0.0002$, both achieving FID scores just above 16, while the highest scores (worst performance) occur around $\tau = 0.002$. In general, the flat trend suggests that τ has a limited effect on GAN performance in this setup, allowing flexibility in its selection without a major impact on output fidelity.

Figures 2c and 2d show the results of the experiments to evaluate the effect of ϵ and $max_history$ parameters. The charts show only negligible differences between the settings. For the ϵ parameter, we expect its impact to be minimal, as it is effectively offset by the residuals observed between consecutive optimization iterations. As for the $max_history$

parameter, we consider a value of 10 sufficient for this dataset to accurately estimate the correction to be applied and the resource usage required to execute the experiment.

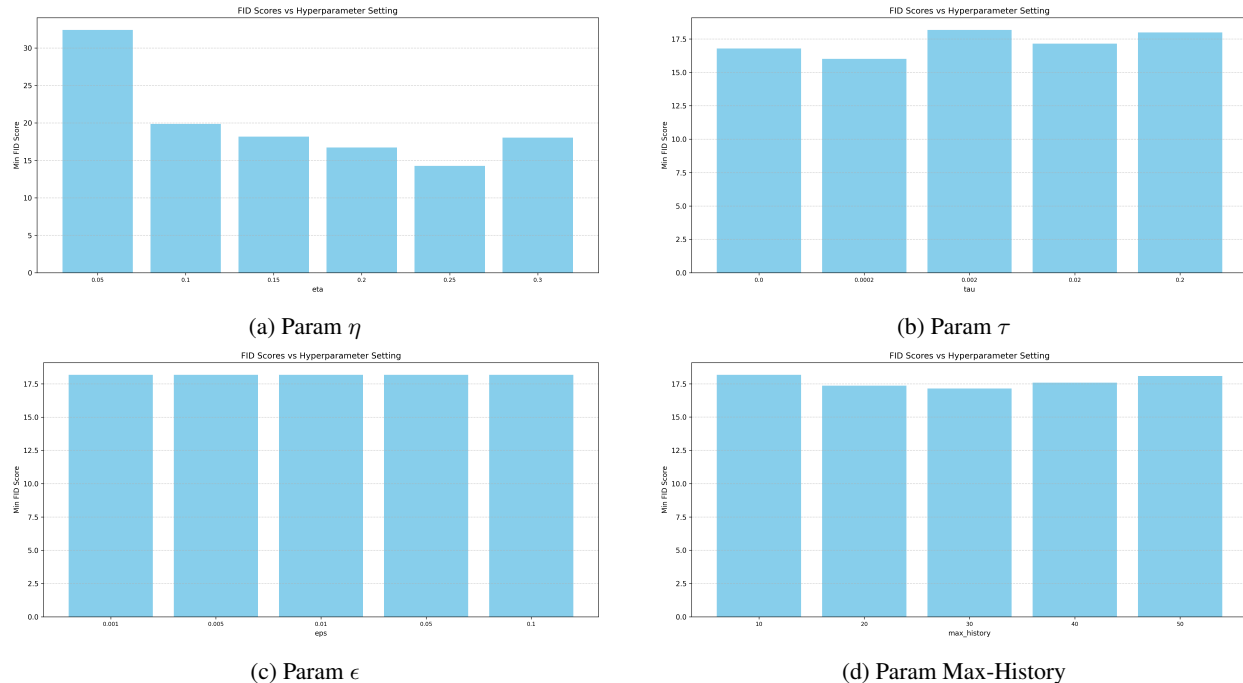


Figure 2: Sensitivity analysis about LM-LRSGAema parameters.

4.2 Experiment on Fashion Mnist

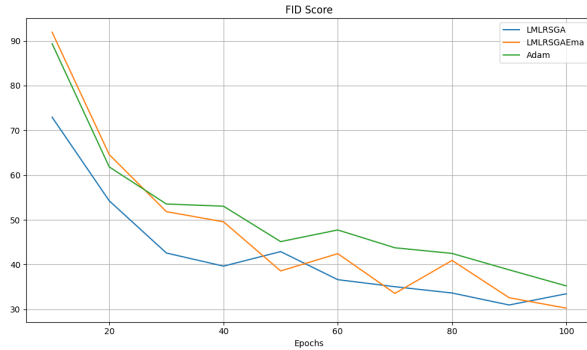
In this section we analyze the results about the Fashion-MNIST dataset, it is a widely used benchmark for image classification tasks, designed as a more challenging drop-in replacement for the original MNIST handwritten digits. It consists of 70,000 grayscale images of size 28×28 pixels, split into 60,000 training samples and 10,000 test samples. We used only the training split to train the GAN models. Each image depicts a single fashion item from one of 10 categories, including T-shirts, trousers, pullovers, dresses, etc. The dataset compact size and diversity make it a standard testbed for evaluating machine learning algorithms in vision research.

Figure 3a shows the evolution of the FID scores over 100 training epochs for the proposed LM-LRSGA and LM-LRSGAema optimizer and the Adam baseline optimizer on the Fashion dataset. The FID score decreases sharply for all methods during the initial epochs, dropping from above 90 to approximately 60–65 by epoch 20, with Adam slightly outperforming LM-LRSGAema in this early phase. However, from epoch 30 onward, LM-LRSGAema consistently achieves lower FID scores, and the performance gap increases as training progresses; while the LM-LRSGA achieves best performance across all epochs. In the final epoch, LM-LRSGAema reaches a FID of around 30, compared to Adam’s ~ 35 , and even surpassing LRSGA; indicating higher image fidelity. These results suggest that, while Adam converges rapidly at the start, LM-LRSGAema delivers more stable improvements and better final generative quality.

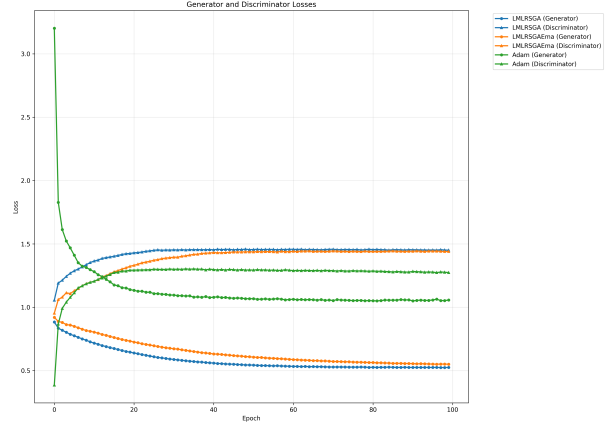
Figure 3b shows the training losses of Adam and LM-LRSGAema. The same behavior of Mnist dataset is observed in this experiment. The two losses converge to a stable value around the epoch ~ 30 for LM-LRSGAema, while Adam converges to some epochs before. The distance between the two losses confirms the ability of LM-LRSGAema to better deal than Adam.

5 Spectral and Stability Analysis

To complement the quantitative evaluation based on FID, we provide an empirical characterization of the dynamical stability of the adversarial training process. We first describe the spectral framework and the quantitative metrics adopted for the analysis, then present the experimental setup and the main results.



(a) FID scores on Fashion dataset.



(b) Training losses on Fashion dataset.

Figure 3: Comparison of LRSGA, LM-LRSGAEmA, and Adam optimizers on Fashion datasets.

5.1 Spectral and Stability Metrics

The spectral and stability analysis relies on an empirical estimation of the local Jacobian of the joint generator–discriminator dynamics, following the theoretical framework for differentiable games introduced in Mescheder et al. [2018], Balduzzi et al. [2018], Fiez and Ratliff [2021]. The procedure combines dimensionality reduction, spectral decomposition, and power–spectral analysis to characterize the linearized dynamics near equilibrium.

Jacobian spectrum estimation. Given the temporal sequence of parameter vectors $w_k = [\theta_G^{(k)}, \theta_D^{(k)}]^\top \in \mathbb{R}^{m+n}$, the discrete dynamics are approximated locally by a linear operator $w_{k+1} \approx Aw_k$, where A is obtained by solving a least-squares regression between successive iterates. To improve conditioning and isolate the dominant modes of variation, the trajectories are projected onto a reduced subspace using truncated Singular Value Decomposition (SVD). This projection corresponds to the standard low-rank approximation $X \approx U_r \Sigma_r V_r^\top$, which filters numerical noise and captures the principal components of the joint update. The reduced operator $A^* = (Y V_r) \Sigma_r^{-1} U_r^\top$ is then analyzed through an eigendecomposition performed via a block-Lanczos iterative scheme, which allows an efficient approximation of the leading eigenvalues without explicitly forming dense matrices. The eigenvalues $\{\lambda_i\}$ of A^* provide an empirical estimate of the local Jacobian spectrum, and the *spectral radius* is defined as $\rho = \max_i |\lambda_i|$.

Stability regime classification. The notions of *stable*, *marginally stable*, and *unstable* dynamics follow the standard classification adopted in the spectral analysis of differentiable and adversarial games Mescheder et al. [2018], Balduzzi et al. [2018], Fiez and Ratliff [2021]. In discrete-time settings, linear stability is determined by the spectral radius of the estimated Jacobian: $\rho < 1$ indicates convergence (stable regime), $\rho = 1$ corresponds to marginal stability, and $\rho > 1$ implies divergence. To account for numerical noise and finite-length trajectories, a tolerance band of $\varepsilon = 0.05$ is applied. Cases with $\rho \in [1 - \varepsilon, 1 + \varepsilon]$ are further analyzed by inspecting the frequency content of the loss trajectories. This inspection is based on the Fourier transform of the temporal loss signals, where the tolerance ε effectively separates slowly varying components from high-frequency oscillatory modes. The spectral energy of the oscillatory band is estimated using *Welch’s method* Welch [1967], which averages modified periodograms over overlapping windows to reduce the variance of the power spectral density (PSD) estimate. If the high-frequency power is small, the dynamics are classified as *marginally stable*; otherwise, the regime is deemed *unstable*. This refinement is consistent with the interpretation of lightly damped rotational dynamics commonly observed in adversarial training systems Fiez and Ratliff [2021].

Auxiliary stability metrics. In addition to the spectral radius, several scalar stability indicators are evaluated to summarize the temporal smoothness and robustness of the optimization process. The *loss stability* index measures the local variability of the generator loss through the inverse of its standard deviation across updates, providing a smoothness score between 0 and 1. The *mode-collapse trend* quantifies the time derivative of the variance of the generator parameters and serves as a proxy for distributional diversity, following the methodology proposed in Lucic et al. [2018]. Finally, the *global stability index* computes the inverse standard deviation of parameter trajectories within sliding windows, functioning as an empirical analogue of a local Lyapunov factor. All metrics are normalized in $[0, 1]$, where larger values indicate smoother and more stable dynamics.

5.2 Experimental Setup

All experiments were conducted on the same MNIST GAN architecture used for the FID evaluation, ensuring full comparability of results. The training dynamics of three optimizers—**Adam**, **LM-LRSGA**, and **LM-LRSGA-EMA**—were analyzed under two *fair* learning-rate regimes:

- (i) **LM-LRSGA-optimal setup**: $\eta = 0.15$, $\tau = 0.002$, corresponding to the FID best-performing configuration for both LM-LRSGA and LM-LRSGA-EMA;
- (ii) **Adam-optimal setup**: $\eta = 0.001$, $\tau = 0.002$, corresponding to the learning rate that maximized the FID performance for Adam.

For each optimizer, the joint trajectories of generator and discriminator parameters were recorded over the entire training process. Parameter updates were collected at uniform intervals and concatenated to form the sequence $w_k = [\theta_G^{(k)}, \theta_D^{(k)}]^\top$. To reduce dimensionality and numerical noise, the trajectories were projected onto a 40-dimensional subspace obtained by truncated SVD. The empirical Jacobian operator was then estimated from these projected trajectories using the least-squares formulation described in Section 5.1. The dominant eigenvalues of the resulting operator were computed through a block-Lanczos iterative decomposition, which efficiently approximates the leading part of the spectrum without constructing dense matrices.

To assess oscillatory behavior, the temporal loss signals of the generator and discriminator were further analyzed in the frequency domain. The power spectral density (PSD) was estimated using *Welch’s method* Welch [1967], as implemented in the `scipy.signal` module. High-frequency power was integrated beyond a cutoff threshold to quantify the spectral energy of oscillations. This quantity was used as a secondary indicator to distinguish marginally stable from unstable regimes in cases where $\rho \approx 1$.

A tolerance parameter of $\varepsilon = 0.05$ was adopted in all experiments for the stability classification, as discussed in Section 5.1. All analyses were performed using Python 3.10 with the NumPy, SciPy, and PyTorch libraries.

5.3 Results and Discussion

Figures 4 and 5 provide a comprehensive visualization of the spectral and stability diagnostics obtained for the analyzed optimizers. The first row reports the evolution of the generator and discriminator losses shown on a logarithmic scale (left), the corresponding training stability metric (center), and the estimated spectrum of the local Jacobian in the complex plane (right). The spectral plot displays the eigenvalues computed from the block-Lanczos approximation of the empirical Jacobian, with the dashed unit circle indicating the boundary between contractive and divergent dynamics. The second row shows the evolution of the generator parameters (left) and discriminator parameters (center), represented by the Euclidean distance from their initialization, and the *mode-collapse indicator* (right). A nearly monotonic decrease of these distances together with a slow, smooth decay of the variance indicates stable and non-collapsing behavior. Overall, the combined diagnostics reveal that both LM-LRSGA variants maintain bounded losses, regular parameter trajectories, and eigenvalues concentrated within or near the unit circle, in contrast to the divergent and oscillatory dynamics observed with Adam.

In particular, the results reported in Table 1 show that when the learning rate was set to the LM-LRSGA-optimal configuration ($\eta = 0.15$, $\tau = 0.002$), **Adam** exhibited a **spectral radius of $\rho = 2.81$** , indicating a strongly divergent regime characterized by high-frequency oscillations and large-amplitude loss fluctuations. The Fourier spectra estimated through Welch’s method Welch [1967] confirmed a concentration of power in the high-frequency range, consistent with unstable dynamics. In contrast, both **LM-LRSGA** and **LM-LRSGA-EMA** maintained nearly marginal stability with $\rho \approx 1.12$ and $\rho \approx 1.14$, respectively. Both optimizers exhibited almost constant global stability indices (≈ 0.99) and parameter oscillations of order $\mathcal{O}(10^{-4})$, with negligible generator variance drift ($\hat{\sigma}_G^2 \approx 0$), confirming the absence of mode collapse and aligning with the superior FID results previously observed.

Across both learning-rate regimes, the limited-memory variants substantially reduce the spectral radius—by approximately **50% relative to Adam**—and maintain stable trajectories even for large step sizes. The reduction of ρ and the absence of high-frequency energy in the loss spectra confirm that the LM-LRSGA correction effectively damps the antisymmetric component of the gradient field, yielding dynamics that are nearly contractive in the sense of the spectral criterion. These findings provide a consistent spectral explanation for the smoother convergence and improved sample quality obtained by LM-LRSGA in the FID experiments.

Table 1: Spectral and stability metrics for Adam, LM-LRSGA, and LM-LRSGA-EMA under two learning-rate regimes. All quantities are computed from block-Lanczos spectral estimates and the auxiliary stability indices described in Section 5.1.

Setting	Optimizer	ρ	Pred. Stab.	Stab. (G/D)	Mode-Collapse
$\eta = 0.15, \tau = 0.002$	Adam	2.81	Unstable	0.30 / 0.72	High
	LM-LRSGA	1.11	Marginal	0.99 / 0.99	Low
	LM-LRSGA-EMA	1.14	Marginal	0.99 / 0.99	Low
$\eta = 0.001, \tau = 0.002$	Adam	1.48	Unstable	0.99 / 0.98	Low
	LM-LRSGA	1.06	Marginal Stable	1.00 / 1.00	Low
	LM-LRSGA-EMA	1.06	Marginal Stable	1.00 / 1.00	Low

6 Conclusions

This work introduced *Limited-Memory Low-Rank Symplectic Gradient Adjustment* (LM-LRSGA), a scalable optimization framework for differentiable games and competitive learning. Building on symplectic gradient corrections and quasi-Newton approximations, LM-LRSGA retains the stabilizing effect of second-order information while reducing memory and compute via two-loop recursions algorithms. By storing only a short history of curvature pairs, it attains near-second-order stability with first-order-like efficiency.

Our analyses show that LM-LRSGA mitigates the rotational dynamics that typically hinder convergence in adversarial settings. On GAN training with MNIST and Fashion-MNIST, it yields smoother, synchronized loss trajectories, faster convergence, and up to 30% FID improvement over Adam. These results indicate that limited-memory curvature corrections offer a practical balance of stability, efficiency, and scalability for competitive optimization.

Future work will focus on consolidating the theoretical foundations. We aim to develop a more comprehensive analysis for nonconvex and locally monotone regimes, where classical tools are less informative. Such a framework would clarify the role of curvature information and symplectic corrections beyond convex-concave settings and inform adaptive limited-memory strategies for broader classes of differentiable games.

LM-LRSGA also supports sustainable, energy-aware machine learning. By avoiding explicit formation and storage of high-dimensional second-order tensors, it reduces memory transfers and expensive operations—two key drivers of energy use in large-scale training—thereby lowering runtime in line with “green AI” principles. Thus, LM-LRSGA provides a step toward methods that are not only theoretically and numerically robust, but also environmentally sustainable.

Finally, quantifying energy savings from optimization algorithms—both in computational cost and carbon footprint—has become an active research topic Colao et al. [2025], Foglia et al. [2024]. In that spirit, future studies will assess the effective carbon footprint reduction enabled by LM-LRSGA, providing a unified view of its theoretical, computational, and environmental impact.

Acknowledgemnt

This publication was partially funded by the PhD program in Mathematics and Computer Science at University of Calabria, Cycle XXXVIII with the support of a scholarship financed by DM 351/2022 (CUP H23C22000440007), based on the NRPP funded by the European Union.

References

- Martin Arjovsky, Soumith Chintala, and Léon Bottou. Wasserstein gan. 2017. URL <http://arxiv.org/abs/1701.07875>. arXiv:1701.07875.
- A Nystrom M Wiatrak, SV Albrecht. Stabilizing generative adversarial networks: A survey. *arXiv preprint arXiv:1910.00927*, 2019.
- David Balduzzi, Sébastien Racanière, James Martens, Jakob Foerster, Karl Tuyls, and Thore Graepel. The mechanics of n-player differentiable games. In *Proceedings of the 35th International Conference on Machine Learning (ICML)*, pages 354–363, 2018.
- Ian Gemp and Sridhar Mahadevan. Global convergence to the equilibrium of gans using variational inequalities, 2018.

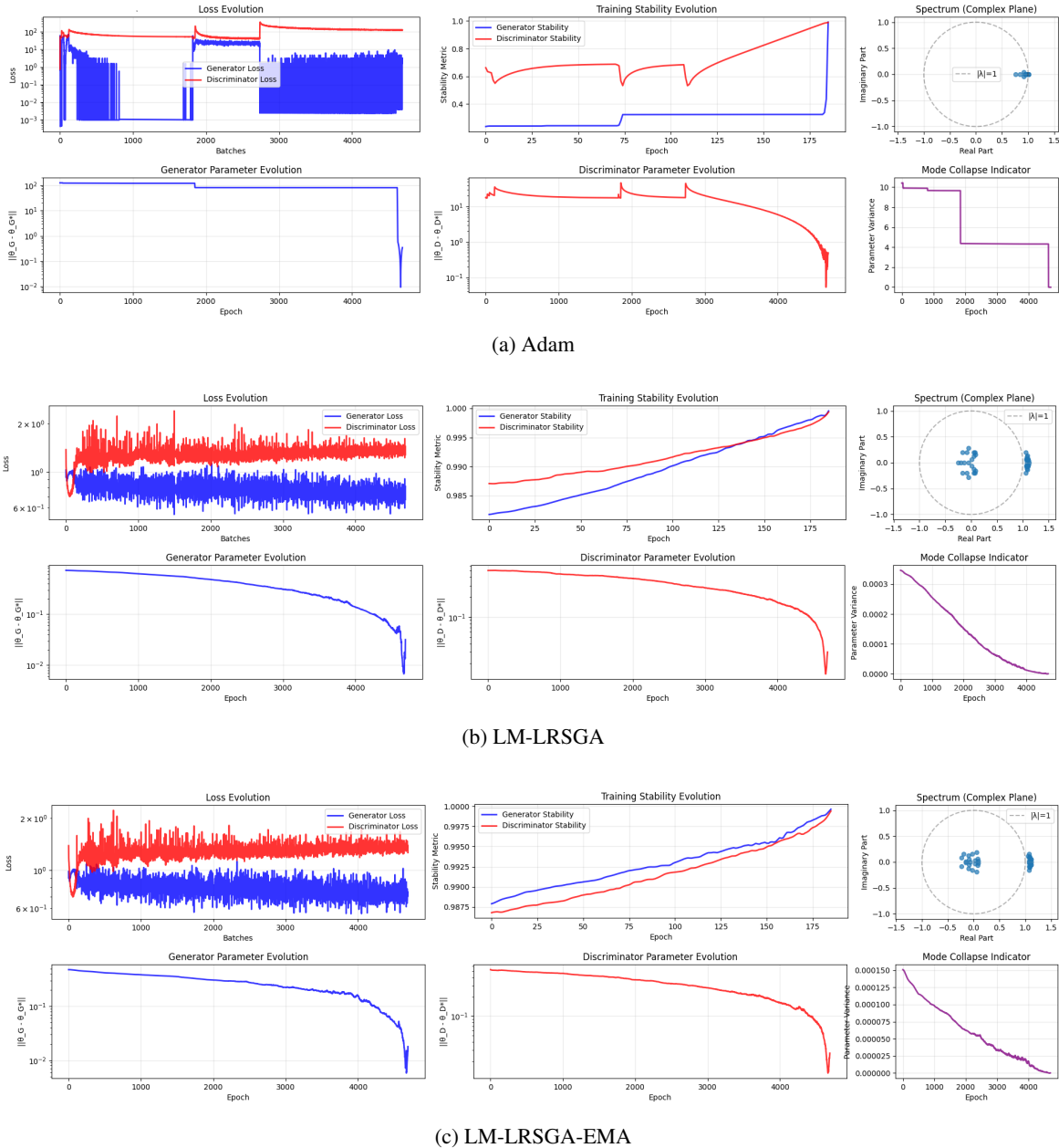


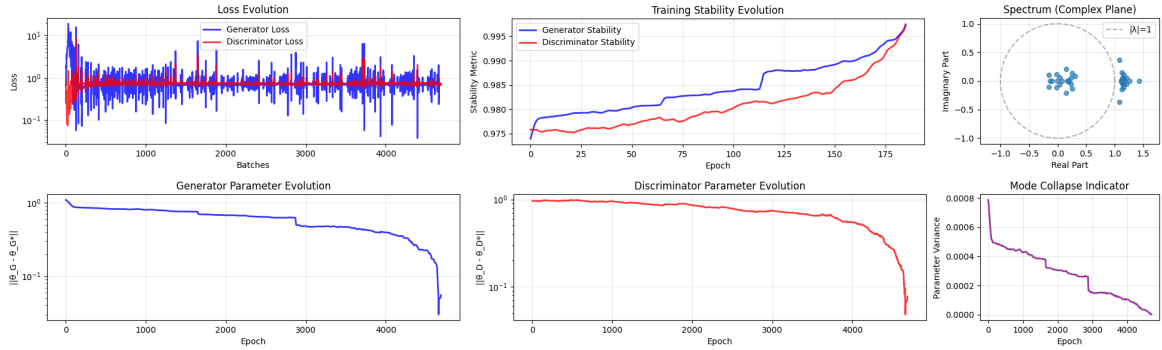
Figure 4: Spectral and stability diagnostics for Adam, LM-LRSGA, and LM-LRSGA-EMA with learning rate $\eta = 0.15$. Each panel shows (top) loss evolution in logarithmic scale, the training stability metric, and the estimated Jacobian spectrum in the complex plane; and (bottom) the generator and discriminator parameter evolution together with the mode-collapse indicator.

Florian Schäfer and Anima Anandkumar. Competitive gradient descent. In *Advances in Neural Information Processing Systems (NeurIPS)*, volume 32, 2019.

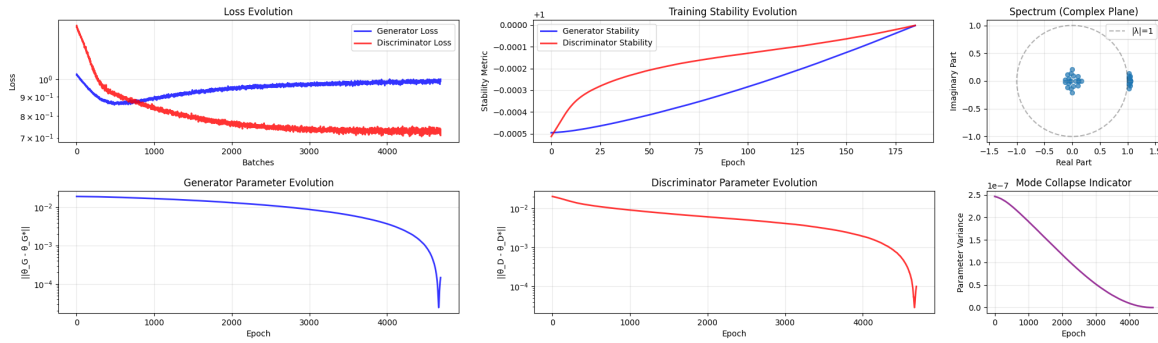
Constantinos Daskalakis and Ioannis Panageas. The limit points of (optimistic) gradient descent in min-max optimization. *Advances in neural information processing systems*, 31, 2018.

Galina M Korpelevich. The extragradient method for finding saddle points and other problems. *Matecon*, 12:747–756, 1976.

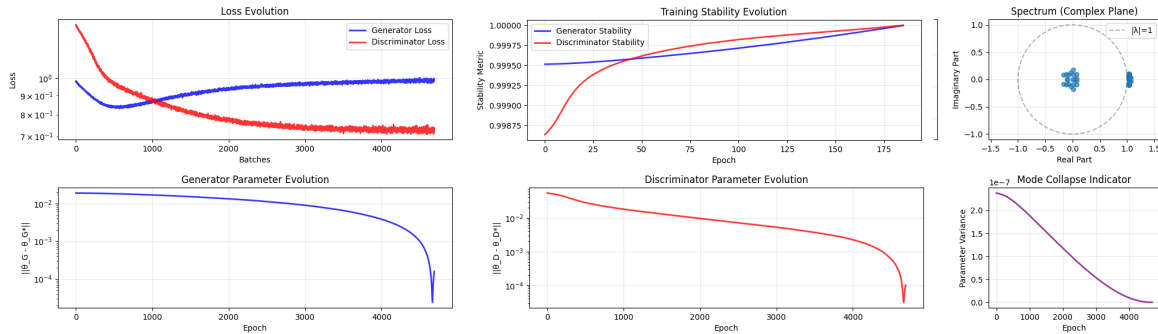
Gauthier Gidel, Hugo Berard, Gaëtan Vignoud, Pascal Vincent, and Simon Lacoste-Julien. A variational inequality perspective on generative adversarial networks. In *International Conference on Learning Representations*, 2019.



(a) Adam



(b) LM-LRSGA



(c) LM-LRSGA-EMA

Figure 5: Spectral and stability diagnostics for Adam, LM-LRSGA, and LM-LRSGA-EMA with learning rate $\eta = 0.001$. Each panel shows (top) loss evolution in logarithmic scale, the training stability metric, and the estimated Jacobian spectrum in the complex plane; and (bottom) the generator and discriminator parameter evolution together with the mode-collapse indicator.

Jorge Nocedal. Updating quasi-newton matrices with limited storage. *Mathematics of Computation*, 35(151):773–782, 1980.

Dong C. Liu and Jorge Nocedal. On the limited memory BFGS method for large scale optimization. *Mathematical Programming*, 45(1–3):503–528, 1989.

Nadja Vater, Katherine R. Foglia, Vittorio Colao, and Alfio Borzì. Low-rank symplectic gradient adjustment for competitive optimization, 2025. Preprint.

Diederik P Kingma and Jimmy Ba. Adam: A method for stochastic optimization. *arXiv preprint arXiv:1412.6980*, 2014.

-
- C. G. Broyden. A class of methods for solving nonlinear simultaneous equations. *Mathematics of Computation*, 19(92): 577–593, 1965.
- Tian-De Guo, Yan Liu, and Cong-Ying Han. An overview of stochastic quasi-newton methods for large-scale machine learning. *Journal of the Operations Research Society of China*, 11(2):245–275, 2023.
- Lars Mescheder, Sebastian Nowozin, and Andreas Geiger. Which training methods for gans do actually converge? In *Proceedings of the 35th International Conference on Machine Learning (ICML)*, pages 3481–3490. PMLR, 2018.
- Tanner Fiez and Lillian J. Ratliff. Spectral analysis of gradient dynamics in multi-agent learning. *SIAM Journal on Control and Optimization*, 59(6):4409–4445, 2021.
- Peter D Welch. The use of fast fourier transform for the estimation of power spectra: A method based on time averaging over short, modified periodograms. *IEEE Transactions on audio and electroacoustics*, 15(2):70–73, 1967.
- Mario Lucic, Karol Kurach, Marcin Michalski, Sylvain Gelly, and Olivier Bousquet. Are GANs created equal? a large-scale study. In *Advances in Neural Information Processing Systems (NeurIPS)*, volume 31, 2018.
- Vittorio Colao, Katherine Rossella Foglia, Andrea Giordano, Ettore Ritacco, and William Spataro. An optimizer derived from halpern’s method for enhanced neural network convergence and reduced carbon emissions. *Journal of Intelligent Information Systems*, pages 1–20, 2025.
- Katherine Rossella Foglia, Vittorio Colao, and Ettore Ritacco. Halpernsgd: A halpern-inspired optimizer for accelerated neural network convergence and reduced carbon footprint. In *International Symposium on Methodologies for Intelligent Systems*, pages 296–305. Springer, 2024.